

Solvable model of quantum Darwinism-encoding transitions

Benoît Ferté¹ and Xiangyu Cao²

¹Université Paris-Saclay, CNRS, LPTMS, 91405, Orsay, France

²Laboratoire de Physique de l'École normale supérieure, ENS, Université PSL, CNRS, Sorbonne Université, Université Paris Cité, F-75005 Paris, France

(Dated: March 13, 2024)

We propose a solvable model of Quantum Darwinism to encoding transitions—abrupt changes in how quantum information spreads in a many-body system under unitary dynamics. We consider a random Clifford circuit on an expanding tree, whose input qubit is entangled with a reference. The model has a Quantum Darwinism phase, where one classical bit of information about the reference can be retrieved from an arbitrarily small fraction of the output qubits, and an encoding phase where such retrieval is impossible. The two phases are separated by a mixed phase and two continuous transitions. We compare the exact result to a two-replica calculation. The latter yields a similar “annealed” phase diagram, which applies also to a model with Haar random unitaries. We relate our approach to measurement induced phase transitions (MIPTs), by solving a modified model where an environment eavesdrops on an encoding system. It has a sharp MIPT only with full access to the environment.

Introduction A pillar of modern quantum statistical mechanics [1–3] is the idea that unitary dynamics in a many-body system generically scrambles local quantum information. Eventually, it becomes highly nonlocal and impossible to retrieve, unless the observer has access to more than half of the system: the information has been encoded [4–7]. Information scrambling and encoding have far-reaching consequences, for example on the quantum physics of black holes [8–13].

Meanwhile, a basic premise of Quantum Darwinism (QD) [14–19] is that a macroscopic environment, e.g., a measurement apparatus, *duplicates* some classical information. Hence, the latter becomes retrievable in multiple small fractions of the environment. It is important to view the environment itself as a many-body quantum system. Indeed, the theory of QD aims to deduce the properties of the classical world from the core principles of quantum physics. According to QD, the duplication of information underlies the emergence of classical *objectivity* [20–23]: being objective is being known to many.

Quantum Darwinism and encoding are distinct ways of many-body quantum information spreading. Both behaviors emerge from the microscopic laws of quantum mechanics, just like both ferro- and para-magnetism can emerge from the Ising model. Ferro- and para-magnetism are distinct phases of matter, separated by a continuous phase transition. Can we view QD and encoding as stable phases of quantum information, and are they separated by some transition [24, 25]? In this Letter, we propose a solvable model of sharp phase transitions from QD to encoding. Our model is a random Clifford unitary circuit on an expanding tree, whose root forms a maximally entangled pair with a reference qubit [Fig. 1-(a)]. It has one parameter, analogue of the temperature in the Ising model. We then ask whether it is possible to retrieve information about the reference bit from a small fraction $f < 1/2$ of the tree’s leaves (output qubits). We deter-

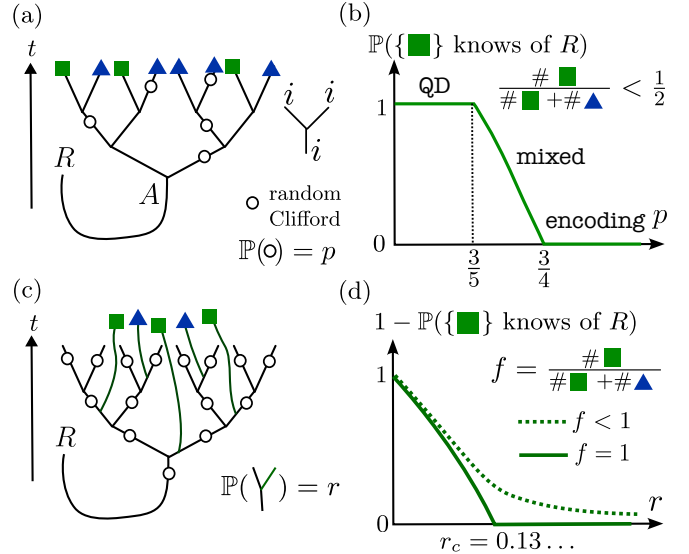


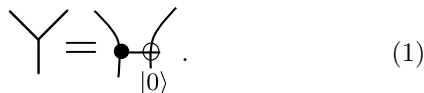
FIG. 1. (a) Model for Quantum Darwinism-encoding transitions on an expanding tree with $t = 3$ generations. (b) Information on R is accessible to a small subsystem (squares) in the Quantum Darwinism (QD) phase, and inaccessible in the encoding phase. In the mixed phase, the information is accessible in a fraction of random realizations. (c) A tree model of an environment eavesdropping on an encoding dynamics. (d) A transition is only possible with full access to the environment $f = 1$.

mine exactly the model’s phase diagram [Fig. 1-(b)]. It has a stable QD (encoding, resp.) phase, where one may (may not, resp.) extract a classical bit of information about the reference bit. Unlike the Ising model, the encoding and QD phases are separated by an intermediate mixed phase and two continuous transitions.

Another inspiration for this work is the measurement-induced phase transitions (MIPT) [26–37], which are also “quantum information transitions”. In the standard

setup, a generic many-body unitary evolution is continually interrupted by local measurements. By tuning the measurement rate, one obtains a transition between a phase with volume-law entanglement entropy and one with area law. The MITPs concern entanglement properties of random states drawn from the Born rule, and are delicate to study and observe [38–40]. Here, we consider a “Darwinian” MITP setup, see Fig. 1-(c,d). We amend our model in the encoding phase with eavesdropping qubits [41], and ask whether they can extract a classical bit of information about the reference [34, 42–45]. We show that a sharp transition occurs at a critical rate of eavesdropping, if and only if one has access to all the eavesdropping bits.

Model for QD-encoding transition Consider a maximally entangled pair $(|0\rangle_R|0\rangle_A + |1\rangle_R|1\rangle_A)/\sqrt{2}$ between a reference qubit R that will be kept intact, and the qubit A that will be the root of an expanding binary tree unitary circuit, see Fig. 1. The edges of the tree represent the world lines of the qubits constituting a growing system [46, 47]. At each branching, we recruit a new qubit with state $|0\rangle$, and apply a CNOT gate to it and the input qubit:



Equivalently, the branching acts on the input qubit as an isometry $\sum_{i=0,1} |ii\rangle\langle i|$. In addition, we apply a random one-body Clifford unitary (drawn uniformly) to each edge of the tree with probability p , which is the parameter that interpolates between the QD ($p = 0$) and encoding limits ($p = 1$). After t time steps, there are $N = 2^t$ output qubits, from which we draw the subsystem F randomly: each output qubit belongs to F with probability f . We denote by U the resulting unitary from A and $N - 1$ recruits to the N output qubits. By construction, U is a Clifford unitary, which can be efficiently simulated [48, 49]. Here, we can analyze the knowledge of F on R analytically [50].

For this, we recall the defining property of a Clifford unitary: it transforms any Pauli operator to a *single* product of Pauli’s, known as a Pauli string. For example, a one-body Clifford unitary permutes X, Y and Z , and choosing a random one-body Clifford amounts to picking one among the 6 permutations (here and below, a Pauli string will be always considered modulo a phase $\pm 1, \pm i$). Now, let us fix a realization of our model, and consider a Pauli string P acting on the subsystem F . By definition, our Clifford unitary U will pull it back to $Q = U^\dagger P U$, a Pauli string acting on A and the $N - 1$ recruits. We then contract it with the recruit states $(|0\rangle\langle 0|)^{\otimes N-1}$ to obtain a Pauli operator O_A acting on A . There are two possibilities: (1) if Q contains an X or Y acting on some recruit bit, O_A vanishes. (2) Otherwise, $O_A \in \{I, Z, X, Y\}$ is identity or a Pauli.

Repeating this for all Pauli strings acting on F , we construct a set $\mathbf{s} \subset \{I, X, Y, Z\}$ of all the nonzero operators O_A thus obtained. It is not hard to see that \mathbf{s} is a subgroup of $\{I, X, Y, Z\}$ (modulo phase), i.e., \mathbf{s} must equal one of these:

$$\begin{aligned} \mathbf{n} &= \{I\}, \mathbf{z} = \{I, Z\}, \mathbf{x} = \{I, X\}, \mathbf{y} = \{I, Y\}, \\ \mathbf{a} &= \{I, Z, X, Y\}. \end{aligned} \quad (2)$$

Since RA is initially a maximally entangled pair, \mathbf{s} tells us exactly what information about R is accessible from F . If $\mathbf{s} = \mathbf{n}$, F is uncorrelated with R . If $\mathbf{s} = \mathbf{z}, \mathbf{x}$ or \mathbf{y} , F contains one classical bit of information on R : some Pauli string O_F on F is perfectly correlated with $O_R = Z, X$ or Y on R . More precisely, $O_F O_R$ is a stabilizer of the output state Ψ_t : $O_F O_R |\Psi_t\rangle = \pm |\Psi_t\rangle$. If $\mathbf{s} = \mathbf{a}$, one may distill from F a qubit maximally entangled with R [50].

Phase diagram The “order parameter” of our model is thus the probability distribution of \mathbf{s} :

$$\pi := (\pi_{\mathbf{n}}, \pi_{\mathbf{z}}, \pi_{\mathbf{x}}, \pi_{\mathbf{y}}, \pi_{\mathbf{a}}), \quad (3)$$

where $\pi_{\mathbf{n}}$ is the probability that $\mathbf{s} = \mathbf{n}$, and so on. We can compute π of a tree with t generations from one with $(t - 1)$ using a “backward recursion” relation. The phase diagram of the model is determined by iterating this relation and analyzing the $t \rightarrow \infty$ limit of π as a function of p (and f) [50]. As a result, we find three phases, see Fig. 1-(b) for a sketch and Fig. 2 for plots. When $p < 3/5$, we have a Quantum Darwinism (QD) phase, where for any $f \in (0, 1)$, we have $\pi_{\mathbf{a}} \rightarrow 0, \pi_{\mathbf{n}} \rightarrow 0$, and

$$\pi_{\mathbf{z}} \rightarrow \frac{3 - 6p + \sqrt{24(p-1)p+9}}{6-6p}, \pi_{\mathbf{x},\mathbf{y}} \rightarrow \frac{1 - \pi_{\mathbf{z}}}{2}. \quad (4)$$

($\pi_{\mathbf{z}} \rightarrow 1$ as $p \rightarrow 0$.) When $p > 3/4$, we have a *encoding* phase, where $\pi_{\mathbf{n}} \rightarrow 1$ if $f < 1/2$ and $\pi_{\mathbf{a}} \rightarrow 1$ if $f > 1/2$. Finally, when $3/5 < p < 3/4$, we have a mixed phase. For any $f < 1/2$, we have $\pi_{\mathbf{a}} \rightarrow 0$ while

$$(\pi_{\mathbf{n}}, \pi_{\mathbf{z}}, \pi_{\mathbf{x}}, \pi_{\mathbf{y}}) \xrightarrow{f < \frac{1}{2}} (1 - u, \frac{u}{2}, \frac{u}{4}, \frac{u}{4}), u = \frac{6 - 8p}{3 - 3p}. \quad (5)$$

Here u is probability that we can retrieve one classical bit from the subsystem F , and it decreases from 1 to 0 as p varies from $3/5$ to $3/4$. The solution for $f > 1/2$ is obtained from (5) by swapping $\pi_{\mathbf{n}}$ and $\pi_{\mathbf{a}}$.

The existence of the two transitions, at $p = 3/5$ and $p = 3/4$ respectively, where π is non-analytical, can be associated to the breaking/restoration of two symmetries of the model. First, a \mathbb{Z}_2 symmetry acts by exchanging $\pi_{\mathbf{n}} \leftrightarrow \pi_{\mathbf{a}}$, or swapping the subsystem F and its complement (without R) [51]. This symmetry is preserved by the circuit dynamics, weakly broken by the “boundary condition” (the choice of F), and restored only in the QD phase. Second, a \mathcal{S}_3 symmetry acts by permuting $\mathbf{x}, \mathbf{y}, \mathbf{z}$ (while leaving \mathbf{n} and \mathbf{a} invariant). This symmetry is preserved by the random one-body Clifford unitary,

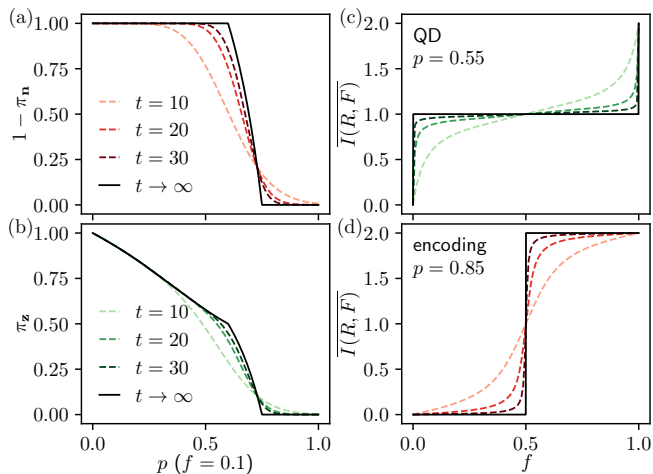


FIG. 2. (a,b) p -dependence of the order parameters $1 - \pi_n$ (identical to Fig. 1-b) and π_z . (c,d) Averaged mutual information $\bar{I}(R, F)$ as a function of the size fraction f in the QD and encoding phase (resp.). The average is over the random Clifford unitary and the random subset F . The finite t data are from numerical iteration of the backward recursion, and the $t = \infty$ curves are the exact prediction [50].

broken by the branching (1), and restored only in the encoding phase. The mixed phase breaks both symmetries. We numerically explored a few other Clifford variants of our model, and found the above two-stage scenario to be rather general [52].

Mutual information and discord It is useful to consider the mutual information between F and R , defined as $I(R, F) = H(R) + H(F) - H(RF)$, where $H(X) = -\text{Tr}[\rho_X \log_2 \rho_X]$ is the von Neumann entropy. In our model, it is not hard to see that $I(R, F) = \log_2 |\mathbf{s}|$ is the dimension of \mathbf{s} as a vector space over \mathbb{Z}_2 [50]. So, in the QD phase,

$$I(R, F) \rightarrow 1 \quad (0 < f < 1) \quad (\text{QD}), \quad (6)$$

with probability one [Fig. 2-(c)]. The independence of I on the fraction size f , sometimes called the “objectivity plateau”, is a hallmark of QD [16]. Meanwhile, in the encoding phase,

$$I(R, F) \rightarrow \begin{cases} 0 & f < 1/2 \\ 2 & f > 1/2 \end{cases} \quad (\text{encoding}) \quad (7)$$

with probability one [Fig. 2-(d)], as expected from the Page curve [53]. In the mixed phase, we may wonder how the I - f curve looks like in a *single* realization (with large t), where we increase f by gradually adding random qubits into F . To address this question, we computed the joint distribution of (\mathbf{s}, \mathbf{t}) corresponding to two random subsystems $F \subset G$, and a same unitary U [50]. As a result, we found that a single-realization I - f curve is exactly the QD one (6) with probability u defined in (5), and exactly the encoding curve (7) with probability

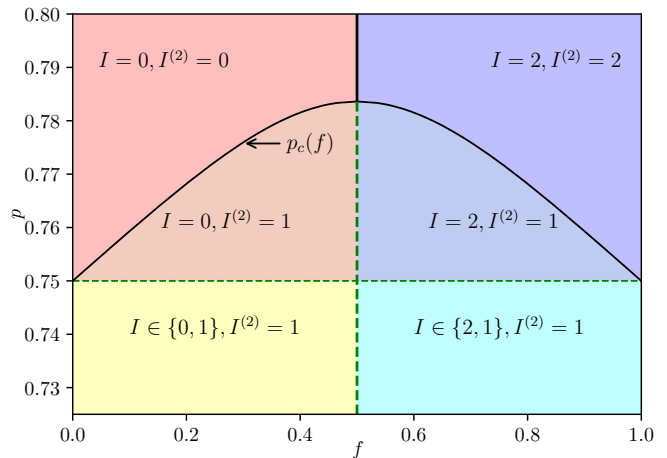


FIG. 3. Comparing the annealed mutual information $I^{(2)}(F, R)$ (9) with the genuine one $I(F, R)$. They disagree in the mixed phase ($3/5 < p < 3/4$) and in part of the encoding phase where $3/4 < p < p_c(f)$. $p_c(f)$ (solid curves) is determined numerically using the recursion relation for $I^{(2)}$ [50].

$1 - u$. In other words, the intermediate-phase ensemble is a mixture of QD and encoding realizations, both occurring with nonzero probability in the $t \rightarrow \infty$ limit.

In general, the mutual information between F and R does not correspond exactly to the amount of information that one can learn about R by observing F [54, 55]. The discrepancy is known as “quantum discord”. Here, the discord vanishes whenever $I(R, F) = 1$, given the knowledge of the unitary circuit: we can construct the observable on F which reveals the classical bit of information on F . Moreover, we can show that in the QD phase, one may still retrieve a bit of information from R even with access to only the Z operators on F .

Two-replica analysis A valuable tool to compute quantum information quantities is the “replica trick” [56–61]. Yet, results of replica calculations can be subtle to interpret, especially if one is not able to take the appropriate replica number limit. Here, we perform a two-replica analysis of our model, and compare the result with the exact phase diagram.

In the replica approach, the accessible quantity is the “annealed” mutual information

$$I^{(2)}(F, R) := \log_2 \text{Tr} \left[\overline{\rho_{FR}^2} \right] - \log_2 \text{Tr} \left[\overline{\rho_F^2} \right] + 1, \quad (8)$$

where $\overline{[\dots]}$ denotes an average over U and F . Note that $I^{(2)}$ would equal to the average von Neumann mutual information if $\text{Tr}[\overline{\rho_X^2}]$ were equal to $2^{-\overline{H(X)}}$ (which is wrong!). The annealed mutual information can be computed by random unitary circuit techniques [37, 51, 62–64]; indeed, since the Clifford group is a 2-design [65], $I^{(2)}(F, R)$ will not change if we replace a random one-body Clifford unitary with a Haar-random one in $U(2)$.

We find [50]:

$$I^{(2)}(F, R) \rightarrow \begin{cases} 0 & f < 1/2, p > p_c(f) \\ 2 & f > 1/2, p > p_c(f) \\ 1 & p < p_c(f) \end{cases}. \quad (9)$$

Here $p_c(f) = p_c(1 - f)$ is a threshold function that increases from $p_c(0) = 3/4$ to $p_c(1/2) = \frac{3}{7}(2\sqrt{2} - 1) = 0.783\dots$, see Fig. 3.

The ‘‘annealed phase diagram’’ of $I^{(2)}$ is similar to the exact one, with however differences: $I^{(2)}(F, R) = 1$ in both QD and mixed phases, as well as a small part of the encoding phase. So, the annealed phase diagram is biased towards QD, which we qualitatively explain as follows. Both purity averages in (8) are dominated by realizations with small entanglement entropy in F . Now, QD states tend to have low entanglement; indeed, the ‘‘perfect’’ QD-state (produced at $p = 0$) is the GHZ state [66],

$$|\text{GHZ}\rangle = \frac{1}{\sqrt{2}}(|0_R \underbrace{0\dots 0}_F 0\dots 0\rangle + |1_R \underbrace{1\dots 1}_F 1\dots 1\rangle).$$

It has one bit of entanglement entropy for any bipartition. In comparison, an encoding state has a volume law entropy. Hence, in both QD and mixed phases, QD realizations will dominate $I^{(2)}$, which fails to distinguish them. In the encoding phase, a QD realization occurs with an exponentially small (in t) probability, yet its $\text{Tr}[\rho_F^2]$ and $\text{Tr}[\rho_{FR}^2]$ can be exponentially large compared to the typical encoding states. Hence, rare QD states in the encoding phase can dominate the annealed mutual information.

Relating to MIPT The QD-encoding transitions (QDETs) differ from the measurement induced ones (MIPTs) in two ways. First, MIPTs result from the competition between a scrambling system and its environment (the measurement apparatus). Meanwhile, QDETs take place within a *structured* environment [67]. In the QD phase, the environment behaves as a macroscopic apparatus that ‘‘measures’’ the reference spin in some direction (the direction is Z with probability π_z , and so on), and broadcast the outcome. As we tune the apparatus into the encoding phase, it becomes dysfunctional and fails to broadcast any information on the reference system.

Second, QDETs are about the information available in small environment fractions, while MIPTs are observable only with full access to the environment. To support this claim, we consider a variant of our model that mimics the MIPT setup. We take the above model at $p = 1$ (in the encoding phase), and let every qubit in the tree be subject to an eavesdropping event with probability r . The eavesdropping consists again as a branching (1), of which one output bit is then emitted to the ‘‘environment’’, see Fig. 1-(c). After t generations, we have a system with $N = 2^t$ bits and an environment E of average size $|E| = (2N - 1)r$.

Then we ask: can we retrieve information on R from a fraction F of the *environment*, with $|F|/|E| = f$? Moreover, we only allow access to Z operators on F (allowing access to all operators results in an entirely different phase diagram [52]). Then, the order parameter (3) obeys a modified recursion relation [50]. In particular, $\pi_a = 0$, and the probability of retrieving one classical bit equals $1 - \pi_n$. We find that, when $f = 1$, there is a transition:

$$\pi_n \xrightarrow{f=1} \begin{cases} \frac{4r^2 - 8r + 1}{1 - r} & r < r_c \\ 0 & r > r_c, \end{cases} \quad (10)$$

where $r_c = \frac{1}{2}(2 - \sqrt{3}) \approx 0.134$. This transition is equivalent to the standard MIPT. Indeed, consider projectively measuring Z on all the qubits of F . If $\mathbf{s} = \mathbf{n}$, the measurements reveal nothing about R , which remains entangled with unmeasured bits. Otherwise, if say $\mathbf{s} = \mathbf{x}$, the measurements will project the qubit R to an eigenstate of X , disentangling it. Therefore, $r > r_c$ is the area-law (purified) phase and $r < r_c$ the volume-law (encoded) phase [34, 42, 44, 45]. Note that the transition exists *only* at $f = 1$, where almost all the environment is accessible. For any $f < 1$, $\pi_n(t \rightarrow \infty)$ depends smoothly on r and never vanishes. This is after all reasonable from the MIPT point of view: we need all the measurement outcomes to construct the quantum trajectory state.

Outlook We introduced a solvable model for Quantum Darwinism-encoding transitions (QDETs). They are a new type of quantum information phase transitions under unitary evolution, where the different phases are characterized by whether information about the reference qubit is retrievable from small fractions of the environment. It will be interesting to identify QDETs in finite-dimensional ($d < \infty$) systems and characterize their universality classes; our tree model is equivalent to an all-to-all ($d = \infty$) circuit, and has simple mean-field critical exponents [68]. In particular, it may be nontrivial to establish a QD phase in a $d < \infty$ geometry, which hinders the fast spread of information [69–71]; an expanding (de Sitter) geometry could be necessary. Another important question concern QDETs in non-Clifford models [24, 41, 72], in particular, whether the mixed phase is generic. Indeed, the knowledge of F on R is in general not ‘‘quantized’’ as in a Clifford model. This will affect the nature of the order parameter, and make even the mean-field theory more involved [46, 47, 73]. Finally, encoding is proper to the quantum realm, and Quantum Darwinism is a theory of the emergence of the classical. Thus, we hope to shed light on the quantum-classical transition through the lens of dynamical critical phenomena.

We thank Andrea De Luca and the Anonymous Referee for helpful comments on the manuscript. X.C. acknowledges support from CNRS and ENS, and thanks LPTMS for hospitality.

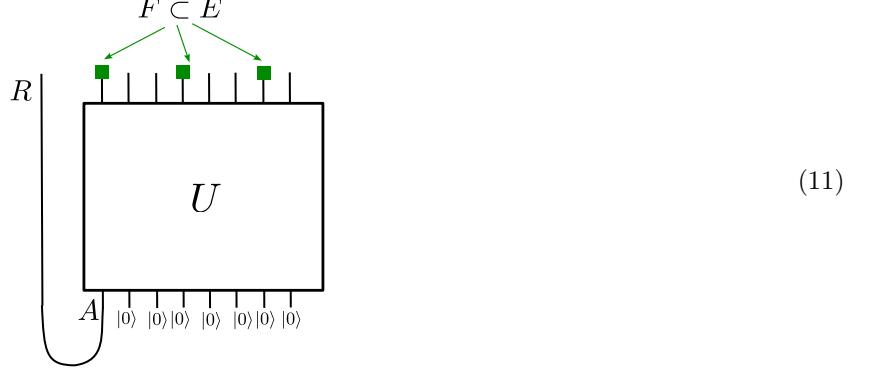
-
- [1] J. M. Deutsch, Quantum statistical mechanics in a closed system, *Phys. Rev. A* **43**, 2046 (1991).
- [2] M. Srednicki, Chaos and quantum thermalization, *Phys. Rev. E* **50**, 888 (1994).
- [3] L. D'Alessio, Y. Kafri, A. Polkovnikov, and M. Rigol, From quantum chaos and eigenstate thermalization to statistical mechanics and thermodynamics, *Advances in Physics* **65**, 239 (2016).
- [4] M. A. Nielsen and I. L. Chuang, *Quantum Computation and Quantum Information: 10th Anniversary Edition* (Cambridge University Press, 2010).
- [5] J. Preskill, *Lecture notes for ph219/cs219: Quantum information* (2023).
- [6] B. Schumacher, Quantum coding, *Phys. Rev. A* **51**, 2738 (1995).
- [7] B. Schumacher and M. D. Westmoreland, Approximate quantum error correction, *Quantum Information Processing* **1**, 5 (2002).
- [8] Y. Sekino and L. Susskind, Fast scramblers, *Journal of High Energy Physics* **2008**, 065 (2008).
- [9] P. Hayden and J. Preskill, Black holes as mirrors: quantum information in random subsystems, *Journal of High Energy Physics* **2007**, 120 (2007).
- [10] S. H. Shenker and D. Stanford, Black holes and the butterfly effect, *Journal of High Energy Physics* **2014**, 67 (2014).
- [11] B. Swingle, Unscrambling the physics of out-of-time-order correlators, *Nature Physics* **14**, 988 (2018).
- [12] A. R. Brown, H. Gharibyan, S. Leichenauer, H. W. Lin, S. Nezami, G. Salton, L. Susskind, B. Swingle, and M. Walter, Quantum gravity in the lab. i. teleportation by size and traversable wormholes, *PRX Quantum* **4**, 010320 (2023).
- [13] T. Schuster, B. Kobrin, P. Gao, I. Cong, E. T. Khabiboulline, N. M. Linke, M. D. Lukin, C. Monroe, B. Yoshida, and N. Y. Yao, Many-body quantum teleportation via operator spreading in the traversable wormhole protocol, *Phys. Rev. X* **12**, 031013 (2022).
- [14] R. Blume-Kohout and W. H. Zurek, Quantum darwinism: Entanglement, branches, and the emergent classicality of redundantly stored quantum information, *Phys. Rev. A* **73**, 062310 (2006).
- [15] H. Ollivier, D. Poulin, and W. H. Zurek, Objective properties from subjective quantum states: Environment as a witness, *Phys. Rev. Lett.* **93**, 220401 (2004).
- [16] W. H. Zurek, Quantum darwinism, *Nature Physics* **5**, 181 (2009).
- [17] M. A. Ciampini, G. Pinna, P. Mataloni, and M. Paternostro, Experimental signature of quantum darwinism in photonic cluster states, *Phys. Rev. A* **98**, 020101 (2018).
- [18] T. K. Uden, D. Louzon, M. Zvolak, W. H. Zurek, and F. Jelezko, Revealing the emergence of classicality using nitrogen-vacancy centers, *Phys. Rev. Lett.* **123**, 140402 (2019).
- [19] W. H. Zurek, Quantum theory of the classical: Einselection, envariance, quantum darwinism and extantons, *Entropy* **24**, 10.3390/e24111520 (2022).
- [20] J. K. Korbicz, P. Horodecki, and R. Horodecki, Objectivity in a noisy photonic environment through quantum state information broadcasting, *Phys. Rev. Lett.* **112**, 120402 (2014).
- [21] T. P. Le and A. Olaya-Castro, Objectivity (or lack thereof): Comparison between predictions of quantum darwinism and spectrum broadcast structure, *Phys. Rev. A* **98**, 032103 (2018).
- [22] T. P. Le and A. Olaya-Castro, Strong quantum darwinism and strong independence are equivalent to spectrum broadcast structure, *Phys. Rev. Lett.* **122**, 010403 (2019).
- [23] J. K. Korbicz, Roads to objectivity: Quantum Darwinism, Spectrum Broadcast Structures, and Strong quantum Darwinism – a review, *Quantum* **5**, 571 (2021).
- [24] C. J. Riedel, W. H. Zurek, and M. Zvolak, The rise and fall of redundancy in decoherence and quantum darwinism, *New Journal of Physics* **14**, 083010 (2012).
- [25] S. Campbell, B. Çakmak, Ö. E. Müstecaplıoğlu, M. Paternostro, and B. Vacchini, Collisional unfolding of quantum darwinism, *Phys. Rev. A* **99**, 042103 (2019).
- [26] B. Skinner, J. Ruhman, and A. Nahum, Measurement-induced phase transitions in the dynamics of entanglement, *Phys. Rev. X* **9**, 031009 (2019).
- [27] Y. Li, X. Chen, and M. P. A. Fisher, Quantum zeno effect and the many-body entanglement transition, *Phys. Rev. B* **98**, 205136 (2018).
- [28] A. Chan, R. M. Nandkishore, M. Pretko, and G. Smith, Unitary-projective entanglement dynamics, *Phys. Rev. B* **99**, 224307 (2019).
- [29] C.-M. Jian, Y.-Z. You, R. Vasseur, and A. W. W. Ludwig, Measurement-induced criticality in random quantum circuits, *Phys. Rev. B* **101**, 104302 (2020).
- [30] X. Cao, A. Tilloy, and A. De Luca, Entanglement in a fermion chain under continuous monitoring, *SciPost Phys.* **7**, 024 (2019).
- [31] M. Sznyszewski, A. Romito, and H. Schomerus, Entanglement transition from variable-strength weak measurements, *Phys. Rev. B* **100**, 064204 (2019).
- [32] Y. Li, X. Chen, and M. P. A. Fisher, Measurement-driven entanglement transition in hybrid quantum circuits, *Phys. Rev. B* **100**, 134306 (2019).
- [33] S. Choi, Y. Bao, X.-L. Qi, and E. Altman, Quantum error correction in scrambling dynamics and measurement-induced phase transition, *Phys. Rev. Lett.* **125**, 030505 (2020).
- [34] Y. Bao, S. Choi, and E. Altman, Theory of the phase transition in random unitary circuits with measurements, *Phys. Rev. B* **101**, 104301 (2020).
- [35] M. J. Gullans and D. A. Huse, Dynamical purification phase transition induced by quantum measurements, *Phys. Rev. X* **10**, 041020 (2020).
- [36] X. Turkeshi, A. Biella, R. Fazio, M. Dalmonte, and M. Schiró, Measurement-induced entanglement transitions in the quantum ising chain: From infinite to zero clicks, *Phys. Rev. B* **103**, 224210 (2021).
- [37] M. P. Fisher, V. Khemani, A. Nahum, and S. Vijay, Random quantum circuits, *Annual Review of Condensed Matter Physics* **14**, 335 (2023).
- [38] Y. Li, Y. Zou, P. Glorioso, E. Altman, and M. Fisher, Cross entropy benchmark for measurement-induced phase transitions, arXiv:2209.00609 10.48550/arXiv.2209.00609 (2022).
- [39] M. Ippoliti and V. Khemani, Postselection-free entanglement dynamics via spacetime duality, *Phys. Rev. Lett.* **126**, 060501 (2021).
- [40] C. Noel, P. Niroula, D. Zhu, A. Risinger, L. Egan, D. Biswas, M. Cetina, A. V. Gorshkov, M. J. Gullans,

- D. A. Huse, and C. Monroe, Measurement-induced quantum phases realized in a trapped-ion quantum computer, *Nature Physics* **18**, 760 (2022).
- [41] A. Touil, B. Yan, D. Girolami, S. Deffner, and W. H. Zurek, Eavesdropping on the decohering environment: Quantum darwinism, amplification, and the origin of objective classical reality, *Phys. Rev. Lett.* **128**, 010401 (2022).
- [42] M. J. Gullans and D. A. Huse, Scalable probes of measurement-induced criticality, *Phys. Rev. Lett.* **125**, 070606 (2020).
- [43] R. Fan, S. Vijay, A. Vishwanath, and Y.-Z. You, Self-organized error correction in random unitary circuits with measurement, *Phys. Rev. B* **103**, 174309 (2021).
- [44] Y. Li and M. P. A. Fisher, Statistical mechanics of quantum error correcting codes, *Phys. Rev. B* **103**, 104306 (2021).
- [45] I. Lovas, U. Agrawal, and S. Vijay, Quantum coding transitions in the presence of boundary dissipation, Preprint [10.48550/arXiv.2304.02664](https://arxiv.org/abs/10.48550/arXiv.2304.02664) (2023).
- [46] A. Nahum, S. Roy, B. Skinner, and J. Ruhman, Measurement and entanglement phase transitions in all-to-all quantum circuits, on quantum trees, and in landau-ginsburg theory, *PRX Quantum* **2**, 010352 (2021).
- [47] X. Feng, B. Skinner, and A. Nahum, Measurement-induced phase transitions on dynamical quantum trees, *PRX Quantum* **4**, 030333 (2023).
- [48] D. Gottesman, The heisenberg representation of quantum computers, Preprint [10.48550/arXiv.quant-ph/9807006](https://arxiv.org/abs/10.48550/arXiv.quant-ph/9807006) (1998).
- [49] S. Aaronson and D. Gottesman, Improved simulation of stabilizer circuits, *Phys. Rev. A* **70**, 052328 (2004).
- [50] See Supplemental Material.
- [51] T. Zhou and A. Nahum, Emergent statistical mechanics of entanglement in random unitary circuits, *Phys. Rev. B* **99**, 174205 (2019).
- [52] Benoît Ferté, Xiangyu Cao, in preparation.
- [53] D. N. Page, Average entropy of a subsystem, *Phys. Rev. Lett.* **71**, 1291 (1993).
- [54] H. Ollivier and W. H. Zurek, Quantum discord: A measure of the quantumness of correlations, *Phys. Rev. Lett.* **88**, 017901 (2001).
- [55] L. Henderson and V. Vedral, Classical, quantum and total correlations, *Journal of Physics A: Mathematical and General* **34**, 6899 (2001).
- [56] C. Holzhey, F. Larsen, and F. Wilczek, Geometric and renormalized entropy in conformal field theory, *Nuclear Physics B* **424**, 443 (1994).
- [57] P. Calabrese and J. Cardy, Entanglement entropy and quantum field theory, *Journal of Statistical Mechanics: Theory and Experiment* **2004**, P06002 (2004).
- [58] P. Calabrese, J. Cardy, and E. Tonni, Entanglement negativity in quantum field theory, *Phys. Rev. Lett.* **109**, 130502 (2012).
- [59] N. Lashkari, Relative entropies in conformal field theory, *Phys. Rev. Lett.* **113**, 051602 (2014).
- [60] J. Zhang, P. Ruggiero, and P. Calabrese, Subsystem trace distance in quantum field theory, *Phys. Rev. Lett.* **122**, 141602 (2019).
- [61] J. Kudler-Flam, Rényi mutual information in quantum field theory, *Phys. Rev. Lett.* **130**, 021603 (2023).
- [62] A. Nahum, J. Ruhman, S. Vijay, and J. Haah, Quantum entanglement growth under random unitary dynamics, *Phys. Rev. X* **7**, 031016 (2017).
- [63] A. Nahum, S. Vijay, and J. Haah, Operator spreading in random unitary circuits, *Phys. Rev. X* **8**, 021014 (2018).
- [64] B. Collins, S. Matsumoto, and J. Novak, The Weingarten Calculus, *Notice of the AMS* **69**, [10.1090/noti2474](https://doi.org/10.1090/noti2474) (2022).
- [65] C. Dankert, R. Cleve, J. Emerson, and E. Livine, Exact and approximate unitary 2-designs and their application to fidelity estimation, *Phys. Rev. A* **80**, 012304 (2009).
- [66] D. M. Greenberger, M. A. Horne, and A. Zeilinger, Going beyond bell's theorem, in *Bell's Theorem, Quantum Theory and Conceptions of the Universe*, edited by M. Kafatos (Springer Netherlands, Dordrecht, 1989) pp. 69–72.
- [67] E. Ryan, M. Paternostro, and S. Campbell, Quantum darwinism in a structured spin environment, *Physics Letters A* **416**, 127675 (2021).
- [68] A. Nahum and K. J. Wiese, Renormalization group for measurement and entanglement phase transitions, *Phys. Rev. B* **108**, 104203 (2023).
- [69] E. H. Lieb and D. W. Robinson, The finite group velocity of quantum spin systems, *Communications in Mathematical Physics* **28**, 251 (1972).
- [70] M. C. Tran, A. Y. Guo, C. L. Baldwin, A. Ehrenberg, A. V. Gorshkov, and A. Lucas, Lieb-robinson light cone for power-law interactions, *Phys. Rev. Lett.* **127**, 160401 (2021).
- [71] C.-F. A. Chen, A. Lucas, and C. Yin, Speed limits and locality in many-body quantum dynamics, *Reports on Progress in Physics* **86**, 116001 (2023).
- [72] R. Blume-Kohout and W. H. Zurek, Quantum darwinism in quantum brownian motion, *Phys. Rev. Lett.* **101**, 240405 (2008).
- [73] B. Ferté and X. Cao, Quantum darwinism-encoding transitions on expanding trees, Preprint [10.48550/arXiv.2312.04284](https://arxiv.org/abs/10.48550/arXiv.2312.04284) (2023).

MODEL OF QUANTUM DARWINISM-ENCODING TRANSITIONS: SOLUTION DETAILS

Clifford-Operator approach to Quantum Darwinism: generalities

In this section we explain in detail our general approach to Quantum Darwinism with Clifford unitary circuits. The results of this section do not depend on the tree structure of the models studied in the main text, and apply to a more general setup, depicted as follows:



where U is any Clifford unitary acting on N qubits. The N input qubits are A , which is maximally entangled to the reference bit R , and the set C of $(N-1)$ recruits that are initialized in a product state $|0\rangle^{\otimes(N-1)}$. For convenience, we shall also denote by U the extended unitary $I_R \otimes U$ that acts trivially on the reference. We would like to understand the correlation between a subset F of the set E of output bits with R .

We start by introducing some notations. Consider a set of qubits X whose size is $|X|$. We shall denote by \mathcal{P}_X the group generated by the Pauli operators acting X ; the elements in \mathcal{P}_X are referred to as *Pauli strings* on X . For example, \mathcal{P}_F is the set of all the (Pauli string) observable to which we have access. The group structure of \mathcal{P}_X is defined by operator multiplication *modulo a phase*. For example, we consider $ZX = Y$ and $ZXZ = X$ to be valid identities, ignoring the factors i and -1 , respectively. (In general, the ignored phases are always a power of i .) Then, $\mathcal{P}_X \simeq \mathbb{Z}_2^{2|X|}$ is isomorphic to the $2|X|$ -dimensional vector space over the finite field with two elements \mathbb{Z}_2 . Hence, we should view \mathcal{P}_X as a vector space.

A state $|\Psi\rangle$ on the qubit set X is a *stabilizer state* if there exists a subspace $\mathcal{S}_\Psi \subset \mathcal{P}_X$ of dimension $|X|$, such that

$$\forall O \in \mathcal{S}_\Psi, O|\Psi\rangle = \pm|\Psi\rangle. \quad (12)$$

The space \mathcal{S}_Ψ is referred to as the *stabilizer space*. It follows that the initial state of the general setup,

$$\Psi_0 = \frac{1}{\sqrt{2}}(|0_R 0_A\rangle + |1_R 1_A\rangle) \prod_{j \in C} |0_j\rangle \quad (13)$$

is a stabilizer state (defined on the qubit set RAC). The stabilizer space is spanned by the following basis:

$$\mathcal{S}_{\Psi_0} = \text{span}(Z_R Z_A, X_R X_A, Z_1, Z_2, \dots, Z_{N-1}) \quad (14)$$

where Z_j acts on the j -th recruit. In particular, as R and A form a maximally entangled pair, Z_R and Z_A are *perfectly correlated*: $Z_R Z_A |\Psi_0\rangle = |\Psi_0\rangle$. The same can be said of X_R and X_A .

By definition, a Clifford unitary U maps any Pauli operator to a Pauli string, and thus determines an isomorphism between the group of Pauli strings on the input and output qubits:

$$\mathcal{U} : \mathcal{P}_{RE} \rightarrow \mathcal{P}_{RAC}, O \mapsto U^\dagger O U. \quad (15)$$

Note that the action of \mathcal{U} is to “pull back” an operator on the output bits to one on the input ones. It follows that the final state $|\Psi_t\rangle := U|\Psi\rangle$ is also a stabilizer state, with the following stabilizer space:

$$\mathcal{S}_{\Psi_t} = \mathcal{U}^{-1} \mathcal{S}_{\Psi_0}. \quad (16)$$

Now, consider the sets of stabilizers supported on F and on RF , $\mathcal{S}_{\Psi_t} \cap \mathcal{P}_F$ and $\mathcal{S}_{\Psi_t} \cap \mathcal{P}_{FR}$, respectively. Both sets are \mathbb{Z}_2 -vector spaces, and the former is contained in the latter. Their dimensions can differ by at most 2, since $\dim(\mathcal{P}_{FR}) - \dim(\mathcal{P}_F) = 2$:

$$\dim(\mathcal{S}_{\Psi_t} \cap \mathcal{P}_{FR}) - \dim(\mathcal{S}_{\Psi_t} \cap \mathcal{P}_F) \in \{0, 1, 2\}. \quad (17)$$

We now come to the first main result: *the above dimension difference equal the mutual information between F and R in the unit of qubits*. Indeed, a classic result on stabilizer states is that the dimension of the stabilizer space \mathcal{S}_X is related to the entanglement entropy (in unit of qubits, with respect to the state Ψ_t) of the subsystem X as follows

$$H(X) = |X| - \dim(\mathcal{S}_{\Psi_t} \cap \mathcal{P}_X), \quad (18)$$

where $|X|$ is the size of X . As a consequence, recalling that $H(R) = 1$, we have:

$$\begin{aligned} I(F, R) &= H(F) + H(R) - H(FR) = |F| - \dim(\mathcal{S}_{\Psi_t} \cap \mathcal{P}_F) + 1 - |FR| + \dim(\mathcal{S}_{\Psi_t} \cap \mathcal{P}_{FR}) \\ &= \dim(\mathcal{S}_{\Psi_t} \cap \mathcal{P}_{FR}) - \dim(\mathcal{S}_{\Psi_t} \cap \mathcal{P}_F). \end{aligned} \quad (19)$$

Furthermore, the quotient space

$$\mathcal{Q} := \frac{\mathcal{S}_{\Psi_t} \cap \mathcal{P}_{FR}}{\mathcal{S}_{\Psi_t} \cap \mathcal{P}_F}, \quad (20)$$

whose dimension equals $I(F, R)$, characterizes more explicitly the correlation between F and R . Let us discuss case by case:

- When $\dim(\mathcal{Q}) = 0$, there is no stabilizer supported on FR that acts non-trivially on R . Thus, we cannot find any Pauli string on F that is perfectly correlated with some non-identity Pauli on R . This is expected from the zero mutual information.
- When $\dim(\mathcal{Q}) = 1$, there is one stabilizer supported on FR acting non-trivially on R . So it takes the form $P_R O_F$, where $P \in \{X, Y, Z\}$ and $O_F \in \mathcal{P}_F$. Therefore, $P_R O|\Psi_t\rangle = \pm|\Psi_t\rangle$ and thus O_F and P_R are perfectly correlated¹. Also, since $\dim(\mathcal{Q}) = 1$, two nonzero representatives of the quotient must differ by a stabilizer in F . Hence the Pauli P_R is unique: there can be perfect correlation between some Pauli string in F and one and only one Pauli on R .
- Finally $\dim(\mathcal{Q}) = 2$ means that we can have two stabilizers $Z_R O_F$ and $X_R O'_F$. They must commute, so O_F and O'_F must anti-commute, and can be viewed as the Z and X operators of some logical qubit. We have thus distilled a qubit from F that is maximally entangled with R , as expected from $I(F, R) = 2$.

So far we have been focusing on the output qubits. The discussion is conceptually straightforward, but computationally inconvenient, since \mathcal{S}_{Ψ_t} is cumbersome to describe directly. To overcome this, we shall use the isomorphism \mathcal{U} (15) to pull back the quotient \mathcal{Q} to the input bits. Using (16) and the fact that U acts trivially on R , we have

$$\mathcal{U}(\mathcal{Q}) = \frac{\mathcal{U}(\mathcal{S}_{\Psi_t} \cap \mathcal{P}_{FR})}{\mathcal{U}(\mathcal{S}_{\Psi_t} \cap \mathcal{P}_F)} = \frac{\mathcal{S}_{\Psi_0} \cap \mathcal{U}(\mathcal{P}_{FR})}{\mathcal{S}_{\Psi_0} \cap \mathcal{U}(\mathcal{P}_F)} = \frac{\mathcal{S}_{\Psi_0} \cap (\mathcal{U}(\mathcal{P}_F) + \mathcal{P}_R)}{\mathcal{S}_{\Psi_0} \cap \mathcal{U}(\mathcal{P}_F)}. \quad (21)$$

Now, recall that \mathcal{S}_{Ψ_0} is explicitly known (14):

$$O \in \mathcal{S}_{\Psi_0} \text{ if and only if } O = O_R O_A \prod_{j \in C} Z_j^{e_j} \quad (22)$$

for some $O \in \{I, X, Y, Z\}$ and $(e_j) \in \{0, 1\}^C$. We now claim that the pull-backed quotient is isomorphic to the ‘‘accessible subspace’’ \mathfrak{s} described in the main text, and of which a formal definition is the following:

$$\mathfrak{s} := \{O_A \in \mathcal{P}_A \mid O_A = \text{Tr}_C[\rho_C \mathcal{U}(O_F)] \text{ for some } O_F \in \mathcal{P}_F\} \quad (23)$$

Here $\rho_C = \prod_{j \in C} |0_j\rangle\langle 0_j|$ is the initial density matrix of the recruits set C and Tr_C is the partial trace on C . To show that claim, consider the linear map

$$\iota : \mathcal{S}_{\Psi_0} \cap (\mathcal{U}(\mathcal{P}_F) + \mathcal{P}_R) \ni O = O_R O_A \prod_{j \in C} Z_j^{e_j} \mapsto O_A \in \mathcal{P}_A. \quad (24)$$

¹ O cannot be identity; otherwise, we would have found a stabilizer

supported on R , contradicting $H(R) = 1$.

Finally u is a one-qubit Clifford gate. It is equal to identity with probability $1 - p$ and randomly chosen from the one-qubit Clifford group with probability p .

It follows that \mathbf{s} can be obtained rather simply from $\mathbf{s}_l = \mathbf{s}(V_l, F_l)$ and $\mathbf{s}_r = \mathbf{s}(V_r, F_r)$, where F_l and F_r are the set of accessible environment bits in the left and right subtree, respectively. More explicitly, we have

$$\mathbf{s} = \sigma_u(\mathbf{B}(\mathbf{s}_l, \mathbf{s}_r)). \quad (32)$$

Here,

- σ_u in (32) implements the pull back action of the one-body Clifford gate:

$$\sigma_u(\mathbf{s}') := \{u^\dagger O u : O \in \mathbf{s}'\}. \quad (33)$$

If u is identity, $\sigma_u(\mathbf{s}') = \mathbf{s}'$ is the identity map. If u is a random one-body Clifford, σ_u acts as a random permutation on $\{\mathbf{x}, \mathbf{y}, \mathbf{z}\}$ and leaves \mathbf{n} and \mathbf{a} intact.

- \mathbf{B} implements the pull-back action of the branching isometry (31) on the accessible subsets:

$$\mathbf{B} : (\mathbf{s}_1, \mathbf{s}_2) \mapsto \{\mathcal{B}^\dagger(P_1 \otimes P_2)\mathcal{B} | P_1 \in \mathbf{s}_1, P_2 \in \mathbf{s}_2\} \cap \{I, Z, X, Y\}. \quad (34)$$

To compute it explicitly, we first calculate the map $(P_1, P_2) \mapsto \mathcal{B}^\dagger(P_1 \otimes P_2)\mathcal{B}$. The result is the following table:

	I	Z	X	Y	
I	I	Z	0	0	(35)
Z	Z	I	0	0	
X	0	0	X	Y	
Y	0	0	Y	X	

It follows that the action of the map \mathbf{B} on a pair of sets is given by another table:

B	n	z	x	y	a	(36)
n	n	z	n	n	z	
z	z	z	z	z	z	
x	n	z	x	y	a	
y	n	z	y	x	a	
a	z	z	a	a	a	

The recursion relation above applies whenever the tree has at least one branching ($t > 0$). The initial case ($t = 0$) is simple: $\mathbf{s} = \mathbf{a}$ if the only leaf of the tree is in F , and $\mathbf{s} = \mathbf{n}$ otherwise.

For a given realization of U and F , we can compute \mathbf{s} by iterating the above recursion relation throughout the whole tree. We start by assigning \mathbf{a} to the leaves in F and \mathbf{n} to those not in F , and then calculate the \mathbf{s} associated with each subtree in a “trickle-down” manner, from the leaves to the root. This is why such a method is known as a “backward recursion”. Here is an illustration, with an arbitrarily chosen realization:



Above, we omitted the \mathbf{n} 's and also wrote the intermediate outputs of the map \mathbf{B} . Also, recall that the absence of a \circ means that the one-body unitary gate is identity, and its trivial action is not written. As a result, we obtain that $I(F, R) = 1$; more precisely, some Pauli string in F is perfectly correlated with the X operator in R .

Backward recursion of the order parameter

The above considerations apply to any fixed realization (F, U) . Now, since the random choices involved in F and U are all made locally (with respect to the tree geometry) and independently, we can perform the average over all the realizations. As a result, we turn the above recursion relation into a recursion map that calculates the probability distribution of \mathbf{s} of a $(t + 1)$ -generation tree, $\pi(t + 1)$, in terms of $\pi(t)$:

$$\pi(t + 1) = M(\pi(t)). \quad (38)$$

Here, the recursion map M is composition of two maps

$$M(\pi) = M_u(M_B(\pi)) \quad (39)$$

that we define now. M_B is a nonlinear map that implements the recursion relation between π 's at a branching, as follows:

$$M_B(\pi)_{\mathbf{s}} = \sum_{\mathbf{s}_1, \mathbf{s}_2} T_{\mathbf{s}_1 \mathbf{s}_2}^{\mathbf{s}} \pi_{\mathbf{s}_1} \pi_{\mathbf{s}_2}, \quad T_{\mathbf{s}_1 \mathbf{s}_2}^{\mathbf{s}} = \begin{cases} 1 & \mathbf{B}(\mathbf{s}_1, \mathbf{s}_2) = \mathbf{s} \\ 0 & \text{otherwise.} \end{cases} \quad (40)$$

Explicitly, we have

$$\begin{bmatrix} M_B(\pi)_{\mathbf{n}} \\ M_B(\pi)_{\mathbf{z}} \\ M_B(\pi)_{\mathbf{x}} \\ M_B(\pi)_{\mathbf{y}} \\ M_B(\pi)_{\mathbf{a}} \end{bmatrix} = \begin{bmatrix} \pi_{\mathbf{n}}^2 + 2\pi_{\mathbf{n}}(\pi_{\mathbf{x}} + \pi_{\mathbf{y}}) \\ \pi_{\mathbf{z}}^2 + 2\pi_{\mathbf{z}}(\pi_{\mathbf{n}} + \pi_{\mathbf{x}} + \pi_{\mathbf{y}} + \pi_{\mathbf{a}}) + 2\pi_{\mathbf{n}}\pi_{\mathbf{a}} \\ \pi_{\mathbf{x}}^2 + \pi_{\mathbf{y}}^2 \\ 2\pi_{\mathbf{x}}\pi_{\mathbf{y}} \\ \pi_{\mathbf{a}}^2 + 2\pi_{\mathbf{a}}(\pi_{\mathbf{x}} + \pi_{\mathbf{y}}) \end{bmatrix}.$$

M_u is a linear map that accounts for the action of the random one-body Clifford (which exists with probability $1 - p$):

$$M_u(y) = (pP_3 + (1 - p)I_5)y, \quad P_3 = \frac{1}{3} \begin{bmatrix} 3 & & & & \\ & 1 & 1 & 1 & \\ & 1 & 1 & 1 & \\ & 1 & 1 & 1 & \\ & & & & 3 \end{bmatrix}. \quad (41)$$

The recursion relation above is supplemented by the initial condition:

$$\pi(t = 0) = M_u(1 - f, 0, 0, 0, f)^T = (1 - f, 0, 0, 0, f)^T. \quad (42)$$

Indeed, a leaf belong to F with probability f , in which case one has access to all of its Pauli's; otherwise, one has access to none. The map M_u is applied since a random Clifford unitary can be applied to the output qubits; yet, this turns out to have no effect on the initial condition of the backward recursion. The recursion map M defines a dynamical system on a space of dimension 4 defined by the sum rule

$$\pi_{\mathbf{n}} + \pi_{\mathbf{z}} + \pi_{\mathbf{x}} + \pi_{\mathbf{y}} + \pi_{\mathbf{a}} = 1, \quad (43)$$

since π is a probability distribution. The phase diagram of the model is determined by the long-time limit of this dynamical system. (It is tempting call the dynamics generated by M the ‘‘renormalization group flow’’ of the model. However we shall refrain from doing that since π 's are not really coupling constants.)

Analysis of the recursion dynamics

In this section we detail the analysis of the recursion dynamics. The results can be summarized as the flow diagrams shown in Figure 4. The method is a combination of analytics and numerics. We find all the fixed points of M (which are the long time limits of π) analytically, as we detail below; we check the fixed points' stability numerically, by diagonalizing the linearization of M around them.

Let us start by discussing the symmetries. First, M preserves the \mathbb{Z}_2 symmetry that swaps \mathbf{n} and \mathbf{a} :

$$M(\tau(\pi)) = \tau(M(\pi)), \text{ where } \tau : (\pi_{\mathbf{n}}, \pi_{\mathbf{z}}, \pi_{\mathbf{x}}, \pi_{\mathbf{y}}, \pi_{\mathbf{a}}) \mapsto (\pi_{\mathbf{a}}, \pi_{\mathbf{z}}, \pi_{\mathbf{x}}, \pi_{\mathbf{y}}, \pi_{\mathbf{n}}). \quad (44)$$

The initial condition (42) breaks this symmetry unless $f = 1/2$; indeed, τ sends f to $1-f$. Another (broken) symmetry of the model is that of \mathcal{S}_3 , which permutes \mathbf{x}, \mathbf{y} and \mathbf{z} and leaves \mathbf{n} and \mathbf{a} intact. This symmetry is preserved by M_u and the initial condition but broken by M_B .

Next, we consider invariant subspaces of the map M . First,

$$I_{xy} := \{\pi : \pi_{\mathbf{x}} = \pi_{\mathbf{y}}\}, \quad (45)$$

is invariant under M and contains the initial conditions, so is where all the dynamics takes place (this can be seen as a ‘‘relic’’ of the broken \mathcal{S}_3 symmetry). Therefore, we shall restrict to I_{xy} in what follows, and reduce the dimension of the dynamical system to 3. It is also useful to note another pair of invariant subspaces,

$$I_+ := \{\pi : \pi_{\mathbf{a}} = 0\}, I_- := \{\pi : \pi_{\mathbf{n}} = 0\}, \quad (46)$$

which are related to each other by the \mathbb{Z}_2 symmetry.

The dynamics $\pi \mapsto M(\pi)$ is structured by the fixed points of M . Indeed, numerically, we do not find any cycle with period > 1 or other nontrivial asymptotic behaviors, and we do not expect these to occur on physical grounds. The fixed points π^* satisfy the following independent equations [we used $\pi_{\mathbf{y}}^* = \pi_{\mathbf{x}}^*$]:

$$3(1 - 2\pi_{\mathbf{x}}^*)\pi_{\mathbf{x}}^* = p \left(2\pi_{\mathbf{n}}^*(\pi_{\mathbf{z}}^* + \pi_{\mathbf{a}}^*) + \pi_{\mathbf{z}}^{*2} + 4\pi_{\mathbf{z}}^*\pi_{\mathbf{x}}^* + 2\pi_{\mathbf{z}}^*\pi_{\mathbf{a}}^* - 2\pi_{\mathbf{x}}^{*2} \right) \quad (47)$$

$$\pi_{\mathbf{a}}^*(\pi_{\mathbf{a}}^* + 4\pi_{\mathbf{x}}^*) = \pi_{\mathbf{a}}^*, \pi_{\mathbf{n}}^*(\pi_{\mathbf{n}}^* + 4\pi_{\mathbf{x}}^*) = \pi_{\mathbf{n}}^*. \quad (48)$$

The last two equations are simple, and allow us to classify the fixed points according their membership with respect to I_+ and I_- .

Outside $I_+ \cup I_-$, there is at most one fixed point. Indeed, such a fixed point must satisfy $\pi_{\mathbf{a}}^* + 4\pi_{\mathbf{x}}^* = \pi_{\mathbf{n}}^* + 4\pi_{\mathbf{x}}^* = 1$, which, combined with the sum rule, gives $\pi_{\mathbf{a}}^* = \pi_{\mathbf{n}}^* = 1 - 4\pi_{\mathbf{x}}^*$, $\pi_{\mathbf{z}}^* = 6\pi_{\mathbf{x}}^* - 1$. (So this fixed point preserves the \mathbb{Z}_2 symmetry.) Plugging these into (47), we obtain a quadratic equation for $\pi_{\mathbf{x}}^*$

$$(6p - 6)\pi_{\mathbf{x}}^{*2} + (3 - 8p)\pi_{\mathbf{x}}^* + p = 0. \quad (49)$$

whose positive solution is

$$\pi_{\mathbf{x}}^* = \frac{-\sqrt{40p^2 - 24p + 9} + 8p - 3}{12(p - 1)}. \quad (50)$$

This solution is physical (i.e. all components π are positive) if and only if $p > 3/5$. When this is the case, the fixed point (50) is always unstable with respect to a \mathbb{Z}_2 -odd perturbation. Indeed, for ϵ small, we have

$$M : (\pi_{\mathbf{a}}^* - \epsilon, \dots, \pi_{\mathbf{n}}^* + \epsilon) \mapsto (\pi_{\mathbf{a}}^* - \lambda\epsilon, \dots, \pi_{\mathbf{a}}^* + \lambda\epsilon) + \mathcal{O}(\epsilon^2),$$

with $\lambda = 1 + \pi_{\mathbf{a}}^* > 1$. Therefore, this fixed point does not characterize a stable phase. Instead, it is the long-time solution for $f = 1/2$ when $p > 3/5$, i.e., along the first-order transition line corresponding to the spontaneous breaking of the \mathbb{Z}_2 symmetry.

We now consider the fixed points in $I_+ \setminus I_-$, i.e., $\pi_{\mathbf{a}}^* = 0$ but $\pi_{\mathbf{n}}^* \neq 0$ (the fixed points in $I_- \setminus I_+$ can be then obtained by applying the \mathbb{Z}_2 symmetry). Then (48) implies $\pi_{\mathbf{n}}^* = 1 - 4\pi_{\mathbf{x}}^*$, and $\pi_{\mathbf{z}}^* = 2\pi_{\mathbf{x}}^*$. Plugging these into (47), we find

$$\pi_{\mathbf{x}}^* \left(\pi_{\mathbf{x}}^* - \frac{3 - 4p}{6(1 - p)} \right) = 0. \quad (51)$$

This gives two fixed points:

$$\pi_* = (1 - u, u/2, u/4, u/4, 0), \quad u = \frac{6 - 8p}{3 - 3p} \text{ or } \pi_* = (1, 0, 0, 0, 0). \quad (52)$$

When $p > 3/4$, only the second one is physical. We checked that it is also stable, and is the long-time limit for any initial condition with $f < 1/2$: this is the encoding phase. When $p \in (3/5, 3/4)$, the fixed point $(1, 0, 0, 0, 0)$ becomes

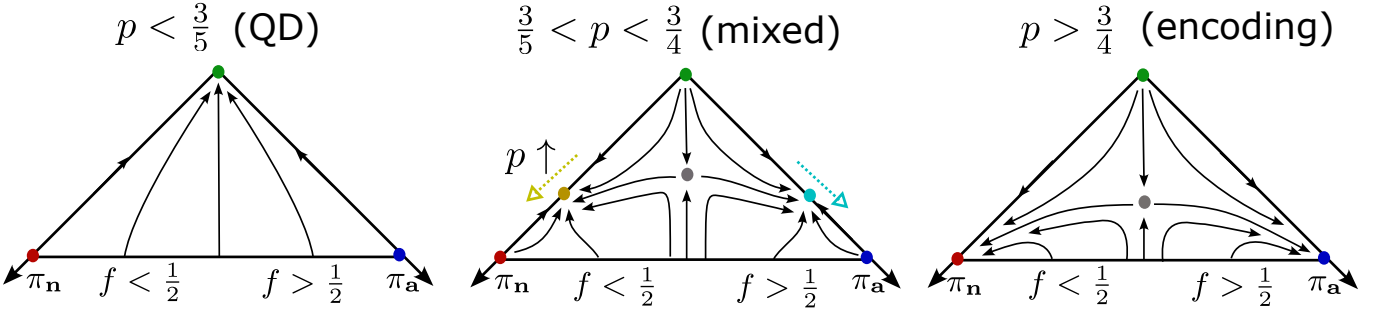


FIG. 4. Flow diagram of the recursion map M in QD, mixed and encoding phases (from left to right), projected onto $\{(\pi_a, \pi_n) : \pi_a \geq 0, \pi_n \geq 0, \pi_a + \pi_n \leq 1\}$. The invariant subspaces I_+ and I_- are projected on the axes. The \mathbb{Z}_2 symmetry acts by a left-right reflection. The initial conditions are at the bottom boundary. The purple fixed point is (50). The yellow fixed point (only existing in the mixed phase) satisfies (51), and the cyan one is related by the \mathbb{Z}_2 symmetry. The yellow and cyan arrows indicate how these fixed points move as p increases.

unstable, and $(1 - u, u/2, u/4, u/4, 0)$ becomes physical, stable and the long-time limit for any initial condition with $f < 1/2$: this is the mixed phase. [When $p < 3/5$, $1 - u < 0$ so $(1 - u, u/2, u/4, u/4, 0)$ is no longer physical.]

Finally, we look at the fixed points in $I_+ \cap I_-$, i.e., with $\pi_a^* = \pi_n^* = 0$. This means that $\pi_z^* = (1 - \pi_z^*)/2$. Plugging into (47), we obtain

$$(3p - 3)\pi_z^{*2} + (3 - 6p)\pi_z^* + p = 0, \quad (53)$$

whose positive solution is given by (4) in the main text:

$$\pi_z^* = \frac{\sqrt{24p^2 - 24p + 9} + 3 - 6p}{6(1 - p)}. \quad (54)$$

This fixed point is always physical, but only stable when $p > 3/5$, and is the long-time limit for any initial condition with $f \in (0, 1)$: this is the QD phase.

We have thus found all the fixed points, and mapped out the phase diagram. In Figure 4 we display the “flow diagrams” of the iteration dynamics in different phases. We remark that each phase is characterized by a unique stable fixed point, modulo the \mathbb{Z}_2 symmetry. Therefore, the long time limit of the recursion dynamics is essentially independent of the initial condition, except when we cross the first-order \mathbb{Z}_2 -breaking transition $\{f = 1/2, p > 3/5\}$. In particular, the initial condition $(1 - f, f, 0, 0, 0)$ results in the same long time limit as $(1 - f, 0, 0, 0, f)$ as long as $f < 1/2$. Physically, this means that in the QD phase, we can retrieve a classical bit of the reference from a small fraction of the system F , even if we can only access the Z operators on F . In the mixed phase, the same can be achieved in a nonzero fraction of the realizations.

Joint distribution

The analysis so far is about the ensemble of (U, F) , i.e., of one random circuit and one random subsystem. To understand the nature of the mixed phase, it is useful to consider the joint ensemble of one random circuit and two random subsystems, (U, F, G) , such that $F \subset G$. They are constructed as follows: for any site i , we determine its membership with respect to F and G independently, with the following probabilities:

$$\mathbb{P}(i \in F) = f, \quad \mathbb{P}(i \in G \setminus F) = g - f, \quad \mathbb{P}(i \notin G) = 1 - g, \quad (55)$$

where $0 < f < g < 1$ are the relative size of F and G , respectively. Note that if we forget about F or G from the joint ensemble, the remaining ensemble is the single subsystem ensemble we studied previously.

For each realization (U, F, G) , we may construct two subgroups \mathbf{s} and \mathbf{t} (of accessible Pauli operators) with respect to F and G , respectively. Then, the order parameter becomes the joint distribution Π of \mathbf{s} and \mathbf{t} , which is a 5×5 matrix (rank 2 tensor). It is straightforward to derive the map M_2 that governs the backward recursion of Π , i.e., the analogue of M (38). Like M , M_2 is a composition of two maps:

$$M_2(\Pi) = M_{2u}(M_{2y}(\Pi)). \quad (56)$$

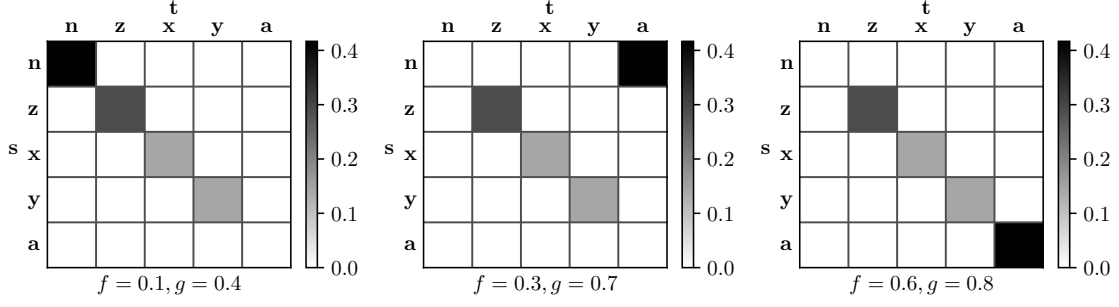


FIG. 5. Examples of the joint distribution $\Pi_{\mathbf{st}}(t \rightarrow \infty)$ in the mixed phase ($p = 0.32$), with different values of f and g , obtained by solving numerically (56)-(58) (one halts the iteration when a fixed point is reached up to numerical precision). One observes that \mathbf{s} and \mathbf{t} are always perfectly correlated, in the way described in text.

Here, M_{2B} is the tensor square of M_B (40):

$$[M_{2B}(\Pi)]_{\mathbf{st}} = \sum_{\mathbf{s}_1 \mathbf{s}_2 \mathbf{t}_1 \mathbf{t}_2} T_{\mathbf{s}_1 \mathbf{s}_2}^{\mathbf{s}} T_{\mathbf{t}_1 \mathbf{t}_2}^{\mathbf{t}} \Pi_{\mathbf{s}_1 \mathbf{t}_1} \Pi_{\mathbf{s}_2 \mathbf{t}_2}. \quad (57)$$

M_{2u} is a linear map $\mathbb{R}^5 \otimes \mathbb{R}^5 \rightarrow \mathbb{R}^5 \otimes \mathbb{R}^5$ defined as follows:

$$M_{2u} = (1-p) I_5 \otimes I_5 + \frac{p}{6} \sum_{\sigma \in S_3} \text{diag}(1, \sigma, 1) \otimes \text{diag}(1, \sigma, 1),$$

where σ is summed over all permutation matrices of size 3, and $\text{diag}(1, \sigma, 1)$ denotes a block diagonal matrix with two blocks of size one (acting on \mathbf{n} and \mathbf{a}) and a block of size 3 (acting on $\mathbf{z}, \mathbf{x}, \mathbf{y}$). Note that M_{2u} is *not* the tensor square of M_u , since the *same* random permutation acts on the two “replicas” with subsystems F and G . The initial condition for Π satisfies

$$\Pi(t=0)_{\mathbf{nn}} = 1-g, \quad \Pi(t=0)_{\mathbf{na}} = g-f, \quad \Pi(t=0)_{\mathbf{aa}} = f, \quad (58)$$

and all the other components are zero.

We studied numerically the recursion relation defined above in the mixed phase ($1/4 < p < 2/5$). For all parameters (p, f, g) tested, we found that $\Pi_{\mathbf{st}}$ has a nonzero limit only in one of the following situations (see Fig. 5 for an example):

- $\mathbf{s} = \mathbf{t} \in \{\mathbf{x}, \mathbf{y}, \mathbf{z}\}$,
- $\mathbf{s} = \mathbf{t} = \mathbf{n}$, and $f < g < 1/2$;
- $\mathbf{s} = \mathbf{t} = \mathbf{a}$, and $1/2 < f < g$;
- $\mathbf{s} = \mathbf{n}, \mathbf{t} = \mathbf{a}$, and $f < 1/2 < g$.

The nonzero values of $\Pi_{\mathbf{st}}$ are completely determined by the fact that the marginal distributions must be equal to the one-point distribution π studied above. Therefore, if we take a single mixed-phase realization in the $t \rightarrow \infty$ limit, and gradually increase the subsystem size fraction f , one and only one of the following scenario will take place:

- We have a “encoding-like” realization in which $\mathbf{s} = \mathbf{n}$ as long as $f < 1/2$, and changes abruptly to $\mathbf{s} = \mathbf{a}$ for $f > 1/2$.
- We have a “QD-Z” realization in which $\mathbf{s} = \mathbf{z}$ for all $0 < f < 1$.
- We have a “QD-X” or “QD-Y” realization, similarly defined.

In short, the mixed-phase ensemble is a macroscopic mixture of encoding-like realizations and QD-like ones. “Intermediate realizations” cannot occur at the $t \rightarrow \infty$ limit, as the two-replica analysis would have suggested (see below).

Model with eavesdropping

The above approach can be used to analyze the model with eavesdropping environment, upon making two modifications. First, the initial condition should be modified to

$$[\pi_{\mathbf{n}}, \pi_{\mathbf{z}}, \pi_{\mathbf{x}}, \pi_{\mathbf{y}}, \pi_{\mathbf{a}}](t=0) = [1, 0, 0, 0, 0], \quad (59)$$

since we have no access to the “system” output bits. Second, the recursion map M is replaced by \tilde{M} , defined as

$$\tilde{M}(\pi) := (1-r)M_{p=1}(\pi) + rM_e(M_{p=1}(\pi)), \quad (60)$$

where

$$M_e(\pi)_{\mathbf{s}} = \sum_{\mathbf{s}_1, \mathbf{s}_2} T_{\mathbf{s}_1 \mathbf{s}_2}^{\mathbf{s}} \pi_{\mathbf{s}_1} \eta_{\mathbf{s}_2}, \quad \eta = [1-f, f, 0, 0, 0], \quad (61)$$

implements the eavesdropping [T is defined in (40)]. Explicitly,

$$M_e(\pi) = f[0, 1, 0, 0, 0]^T + (1-f)[\pi_{\mathbf{n}} + \pi_{\mathbf{x}} + \pi_{\mathbf{y}}, \pi_{\mathbf{z}} + \pi_{\mathbf{a}}, 0, 0, 0]^T. \quad (62)$$

To analyze the asymptotic behavior \tilde{M} , we first realize that the recursion dynamics is confined in the two-dimensional subspace

$$I_{xy} \cap I_+ = \{\pi_{\mathbf{a}} = 0, \pi_{\mathbf{x}} = \pi_{\mathbf{y}}, \pi_{\mathbf{z}} = 1 - \pi_{\mathbf{n}} - 2\pi_{\mathbf{x}}\}. \quad (63)$$

The fixed points are determined by two independent equations:

$$\pi_{\mathbf{x}}^* = \frac{1}{3}(1-r)(1 - \pi_{\mathbf{n}}^*(\pi_{\mathbf{n}}^* + 4\pi_{\mathbf{x}}^*)), \quad \pi_{\mathbf{n}}^* = \frac{r}{3}(1-f)(\pi_{\mathbf{n}}^*(\pi_{\mathbf{n}}^* + 4\pi_{\mathbf{x}}^*) + 2) + \pi_{\mathbf{n}}^*(1-r)(\pi_{\mathbf{n}}^* + 4\pi_{\mathbf{x}}^*). \quad (64)$$

One may solve the first equation for $\pi_{\mathbf{x}}^*$ and plug the result into the second, which becomes a quadratic equation:

$$(fr - 2r + 1)\pi_{\mathbf{n}}^{*2} + (4r - 1 + 4fr - 4fr^2)\pi_{\mathbf{n}}^* + 2(f-1)r = 0. \quad (65)$$

We see immediately that $\pi_{\mathbf{n}}^* = 0$ can be a solution if and only if $f = 1$.

When $f = 1$, the other solution of (65)

$$\pi_{\mathbf{n}}^* = \frac{4r^2 - 8r + 1}{1-r} \quad (66)$$

is negative when $r > r_c = \frac{1}{2}(2 - \sqrt{3})$. In this case, $\pi_{\mathbf{n}}^* = 0$ is the only physical fixed point, and $\pi_{\mathbf{n}} \rightarrow 0$ in the $t \rightarrow \infty$ limit: this is the purified phase. When $r < r_c$, (66) becomes a positive fixed point. It is also the only stable one, so $\pi_{\mathbf{n}} \rightarrow (4r^2 - 8r + 1)/(1-r) > 0$: we are in the “volume law” (or encoded) phase where there is nonzero probability that the environment fails to disentangle the reference from the system.

When $f < 1$, (65) always has one and only one positive root, and thus the $t \rightarrow \infty$ limit of $\pi_{\mathbf{n}}$ depends smoothly on f and r . This means that there is no sharp MIPT-like transition if one can only access a fraction of the environment. When f is close to 1 and r close to r_c , the singular part of $\pi_{\mathbf{n}}^*$ has the following single-parameter scaling behavior:

$$\pi_{\mathbf{n}}^* + 4(r - r_c) \sim 4|r - r_c| \mathcal{F} \left((1-f)^{\frac{1}{2}} / |r - r_c| \right), \quad \mathcal{F}(y) = \sqrt{y^2 / (4\sqrt{3}) + 1}. \quad (67)$$

DETAILS OF THE TWO-REPLICA ANALYSIS

We recall that, in general, the purity of a density matrix ρ is equal to the expectation value of the partial swap operator that exchanges the two replicas,

$$\text{Tr}[\rho^2] = \text{Tr}[(\rho \otimes \rho)\text{SWAP}], \quad \text{SWAP}|a\rangle|b\rangle := |b\rangle|a\rangle. \quad (68)$$

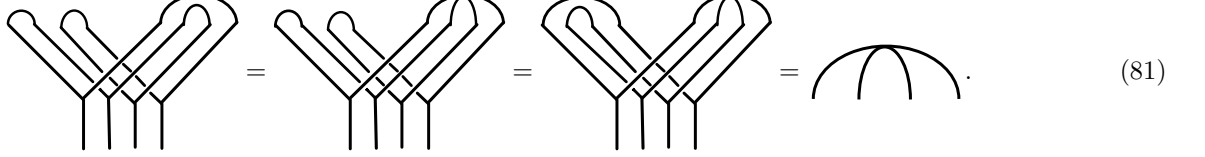
To compute the annealed mutual information $I^{(2)}$, we should take ρ to be the reduced density matrix of the subsystem F or FR . Therefore, our strategy would be to consider the partial swap operator on F , evolve it backward with the

The results for $L_{\mathcal{B}}$ can be summarized in a table

$L_{\mathcal{B}}$	$ \sigma\rangle$	$ \nu\rangle$	$ \tau\rangle$
$ \sigma\rangle$	$ \sigma\rangle$	$ \nu\rangle$	$ \nu\rangle$
$ \nu\rangle$	$ \nu\rangle$	$ \nu\rangle$	$ \nu\rangle$
$ \tau\rangle$	$ \nu\rangle$	$ \nu\rangle$	$ \tau\rangle$

(80)

That is, $L_{\mathcal{B}}$ maps all products between the three states to $|\nu\rangle$ except $|\sigma\rangle|\sigma\rangle \mapsto |\sigma\rangle$, $|\tau\rangle|\tau\rangle \mapsto |\tau\rangle$. The latter cases follow from the fact that \mathcal{B} is an isometry. The other cases can be seen diagrammatically as follows:


(81)

Here, the first three diagrams represent $L_{\mathcal{B}}$ applied to $|\sigma\rangle|\tau\rangle$, $|\sigma\rangle|\nu\rangle$ and $|\tau\rangle|\nu\rangle$, respectively. In each case, the diagram has a single connected component. This forces all the output indices to be equal, which is exactly what $|\nu\rangle$ does.

For L_u , we have

$$L_u|\sigma\rangle = |\sigma\rangle, L_u|\tau\rangle = |\tau\rangle, L_u|\nu\rangle = \frac{1}{3} [|\sigma\rangle + |\tau\rangle]. \quad (82)$$

[If u is averaged over the unitary group $U(q)$, $1/3$ is replaced by $1/(q+1)$.] The first two equations of (82) follow from unitarity, whereas the last one can be derived using the Haar average formula (here $q=2$)

$$\begin{aligned} \left\langle \begin{array}{c} \circlearrowleft \\ u \\ \circlearrowright \\ u \\ \circlearrowleft \\ u \\ \circlearrowright \\ u \end{array} \right\rangle_{U(q)} &= \frac{1}{q^2-1} \begin{array}{c} \cup \\ \cup \\ \cup \\ \cup \end{array} + \frac{1}{q^2-1} \begin{array}{c} \cup \\ \cup \\ \cup \\ \cup \end{array} \\ &\quad - \frac{1}{q(q^2-1)} \begin{array}{c} \cup \\ \cup \\ \cup \\ \cup \end{array} - \frac{1}{q(q^2-1)} \begin{array}{c} \cup \\ \cup \\ \cup \\ \cup \end{array}, \end{aligned}$$

combined with $\langle \sigma|\nu\rangle = \langle \tau|\nu\rangle = q$ (which can be checked diagrammatically).

Equations (80) and (82) imply that $|\overline{O}(t)\rangle$ is indeed a linear combination as in (78), and that the weights satisfy the recursion relation generated by the map:

$$M_w : \begin{bmatrix} w_\sigma \\ w_\nu \\ w_\tau \end{bmatrix} \mapsto \begin{bmatrix} 1 & \frac{1-p}{3} & 0 \\ 0 & p & 0 \\ 0 & \frac{1-p}{3} & 1 \end{bmatrix} \begin{bmatrix} w_\sigma^2 \\ w_\nu^2 + 2(w_\sigma w_\nu + w_\sigma w_\tau + w_\nu w_\tau) \\ w_\tau^2 \end{bmatrix}. \quad (83)$$

By (77), the initial condition is

$$(w_\sigma(t=0), w_\nu(t=0), w_\tau(t=0)) = (1-f, 0, f). \quad (84)$$

It remains to analyze the asymptotic behavior of the dynamical system generated by M_w . We observe that similarly to the recursion map M above, M_w preserves a \mathbb{Z}_2 symmetry, which acts by exchanging σ and τ ; the new state ν is \mathbb{Z}_2 even. However, there is a crucial difference: unlike M , M_w does not preserve the sum $w_\sigma + w_\nu + w_\tau$. Indeed, $(w_\sigma, w_\nu, w_\tau)$ is not a probability distribution, but rather ‘‘partition functions’’ with different boundary conditions at the root of the tree. Yet, w_σ, w_ν, w_τ are still non-negative. So we shall look for fixed points of M_w up to a global factor. As a result of an elementary analysis, we find the following physically relevant fixed points:

- The ‘‘encoding’’ fixed points $(w_\sigma^*, w_\nu^*, w_\tau^*) \propto (1, 0, 0)$ and $(0, 0, 1)$.
- The ‘‘QD’’ fixed point $(w_\sigma^*, w_\nu^*, w_\tau^*) \propto (u, 1-2u, u)$ where $u = u(p)$ is defined implicitly by inverting

$$p = \frac{3(1-u)u}{(u+1)(1-2u^2)}, \quad (85)$$

and choosing the branch that increases from $u(p=0) = 0$ to $u(p=1) = 1/2$.

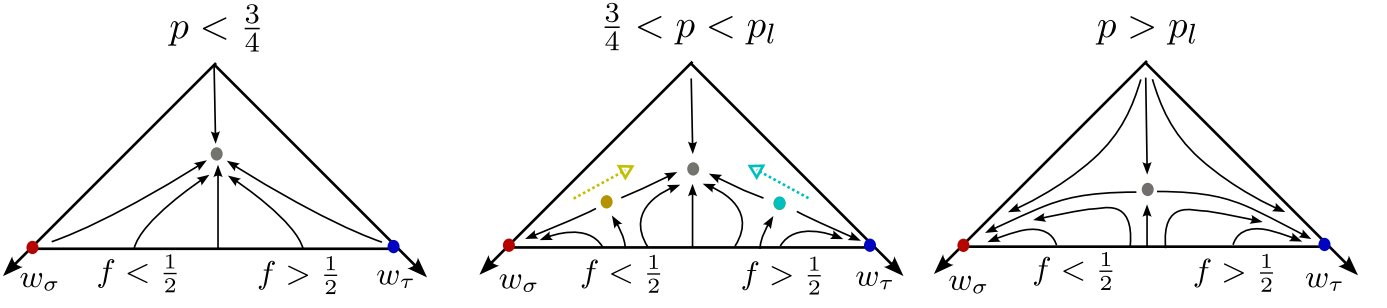


FIG. 6. Flow diagram of the recursion map M_w for $p < 3/4$, $3/4 < p < p_l$ and $p > p_l = \frac{3}{7}(2\sqrt{2}-1)$ (from left to right). We consider $(w_\sigma, w_\nu, w_\tau)$ up to a global factor, and choose to normalize them so that they sum to 1. The grey fixed point is (85). The yellow and cyan fixed points satisfy (86). When they exist, there are two threshold values of f at which the asymptotic limit depends discontinuously on the initial condition. This gives rise to a f -dependent threshold $p_c(f)$, such that $p_c(1/2) = p_l$ and $p_c(0) = p_c(1) = 1/4$. The yellow and cyan arrows indicate how the intermediate fix points move as p increases.

- A pair of intermediate \mathbb{Z}_2 breaking fixed points $(w_\sigma^*, w_\nu^*, w_\tau^*) \propto (u_+, 1 - u_+ - u_-, u_-)$ where u_\pm are the two roots of the equation

$$pu^2 - (3 - 3p)u + 4p - 3 = 0. \quad (86)$$

These fixed points are physical only when $3/4 \leq p \leq p_l$, where

$$p_l = \frac{3}{7}(2\sqrt{2} - 1) \approx 0.783\dots \quad (87)$$

Both fixed points merge with the QD fixed point as $p \nearrow p_l$ and become complex as $p > p_l$. They tend to the encoding fixed points as $p \searrow 3/4$, and become non-positive as $p < 3/4$. (See Figure 6.)

Next we discuss the stability of the fixed points and the phase diagram, see Figure 6 for the flow diagram. The intermediate fixed points are always unstable. The encoding fixed points are stable when $p > 3/4$ and unstable when $p < 3/4$, and the QD fixed point is stable when $p < p_l$ and unstable when $p > p_l$. Therefore,

- When $p > p_l$, w can only tend to the encoding fixed points, $\propto (1, 0, 0)$ if $f < 1/2$ and $\propto (0, 0, 1)$ if $f > 1/2$. This means that $\bar{O} \propto \sigma$ or τ , and $I^{(2)} = 0$ or 2 in the two cases.
- When $p < 3/4$, w can only tend to the QD fixed point, $\propto (u, 1 - 2u, u)$. In this case $\bar{O} \propto u(\sigma + \tau) + (1 - 2u)\nu$, and $I^{(2)} = 1$.
- Finally, when $3/4 < p < p_l$, w may tend to either an encoding or the QD fixed point, depending on the location of initial condition with respect to the stable manifold of the intermediate fixed points. Thus, there is a f -dependent threshold $p_c(f) \in (3/4, p_l)$, such that $I^{(2)} \rightarrow 0$ or 2 if $p > p_c(f)$ and $I^{(2)} \rightarrow 1$ if $p < p_c(f)$. We have not found a closed-form expression of $p_c(f)$, and evaluated it numerically (see Figure 3 of main text). It increases from $3/4$ to p_l as f increase from 0 to $1/2$, and satisfies $p_c(f) = p_c(1 - f)$.

A notable consequence of our two-replica analysis is that the “annealed I - f curve” when $p \in (3/4, p_l)$ is as follows:

$$I^{(2)}(R, F) \rightarrow \begin{cases} 0 & f < 1/2, p > p_c(f) \\ 1 & p < p_c(f) \\ 2 & f > 1/2, p > p_c(f) \end{cases}. \quad (88)$$

It differs from both the QD and encoding I - f curves. Now, if one assumed that $I^{(2)}(R, F)$ equals $\overline{I(R, F)}$, the average of the true mutual information (which is a wrong assumption), then (88) would imply the existence (with nonzero probability as $t \rightarrow \infty$) of realizations whose I - f curves differ from both QD and encoding curves. We have seen from the exact solution above that this is not the case! From the point of view of the flow diagram, the “intermediate” $I^{(2)}$ - f curve (88) occurs because of the existence of the unstable \mathbb{Z}_2 -breaking fixed points. We have not found such fixed points from the replica-free analysis of any (Clifford) variants of our model that we studied (to be reported separately).